Fuel 385 (2025) 134101

Contents lists available at ScienceDirect

Fuel

journal homepage: www.elsevier.com/locate/fuel

Full Length Article

MS_2/TiO_2 (M = Co, Sn and Ni) electrodes for electrocatalytic and photocatalytic water splitting

Sivagowri Shanmugaratnam [a,b,*], Swathi Srinivasan [c], Rathinam Yuvakkumar [c], Velaug Myrseth Oltedal [a], Punniamoorthi Ravirajan [b], Yohi Shivatharsiny [d,e,*], Dhayalan Velauthapillai [a,*]

[a] Faculty of Technology, Environment and Social Sciences, Western Norway University of Applied Sciences, P.O. Box 7030, 5020 Bergen, Norway
[b] Clean Energy Research Laboratory, University of Jaffna, Jaffna 40000, Sri Lanka
[c] Department of Physics, Alagappa University, Karaikudi 630 003, Tamil Nadu, India
[d] Department of Chemistry, University of Jaffna, Jaffna 40000, Sri Lanka
[e] Chemistry and Biochemistry Department, Augustana University, Sioux Falls, SD 57197, USA

ARTICLE INFO

Keywords:
Metal chalcogenides
Hydrothermal
Hydrogen
Electrocatalytic
Photocatalysis

ABSTRACT

Exploring an efficient and stable nanocatalyst for water splitting is a highly desirable, but still a challenging goal. Herein, we synthesized different metalchalcogenides (MS_2: M = Co, Ni, Sn) embedded with TiO_2 that form nanocomposites by the facile hydrothermal method for water splitting. The crystallinity and phases of the prepared materials were confirmed by X-Ray diffractive spectra; the morphology of the particles was studied by Scanning Electron Microscopy; and their superior catalytic performance in electrochemical and photocatalytic activity were examined using electrochemical characterization and photocatalytic experiments, respectively. In electrochemical processes, compared with bare TiO_2, 10 wt% CoS_2/TiO_2, SnS_2/TiO_2, and NiS_2/TiO_2 nanocomposites exhibited high current densities with low Tafel slope values in hydrogen evolution reaction (HER) and oxygen evolution reaction (OER). In addition, the amounts of hydrogen evolution in electrocatalysis and photocatalysis reactions were examined. These results show that metalchalcogenide (MS_2) embedded with TiO_2 nanocomposites electrodes are highly promising candidates to be used as efficient electro and photocatalysts for the water splitting process.

1. Introduction

To reduce greenhouses gases, the research community has been focusing on renewable energy sources. Due to tackle the issue of surplus electricity from renewable energy resources, hydrogen has emerged as a potential candidate for both energy storage and energy transport. In the clean energy mix, hydrogen has a considerable role to play also in number of industries like steal to fertilizer production. High level of energy density and non-polluting characteristics have made hydrogen as one of the most alluring and promising new fuels in the future energy systems [1,2].

There are different hydrogen production methods, such as coal gasification, steam methane reforming, electrolysis, electrochemical method, and photocatalysis. [3]. Currently, a huge amount, roughly 90 %–95 % of hydrogen is produced from coal gasification and stream reforming of natural gases [4]. However, during these processes, hydrogen is produced with greenhouse gases (CO_2, and CO) and referred to as brown and grey hydrogen, respectively. The so-called 'blue hydrogen' is produced through carbon capture and storage during the production process [5,6]. Hydrogen produced without any carbon emissions is referred to as green hydrogen [5,7]. In this process, hydrogen is produced from splitting of water molecule resulting in only hydrogen and oxygen gases as products. There are several green hydrogen production methods categorized as electrolysis, PV-electrolysis [8], electrochemical [9], photoelectrochemical [10] and photocatalysis [11].

Among these, both electrochemical and photocatalytic water splitting methods are the easiest, cost effective, and high purity methods, which produce hydrogen and oxygen without any greenhouse gas emissions [12]. The photocatalysis method is an attractive and efficient technique to produce the hydrogen in the presence of direct sunlight, and it can occur in ambient conditions. In general, photocatalytic

* Corresponding authors.

https://doi.org/10.1016/j.fuel.2024.134101
Received 9 October 2024; Received in revised form 2 December 2024; Accepted 11 December 2024
Available online 14 December 2024

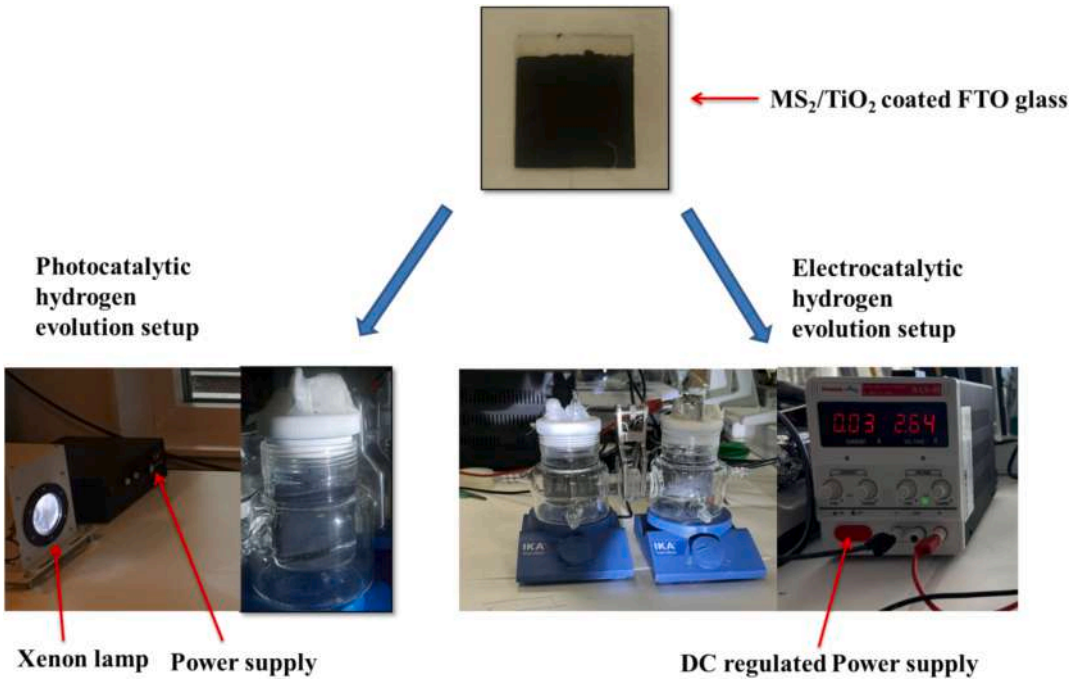

Fig. 1. Photocatalytic and electrocatalytic Hydrogen evolution experimental setup.

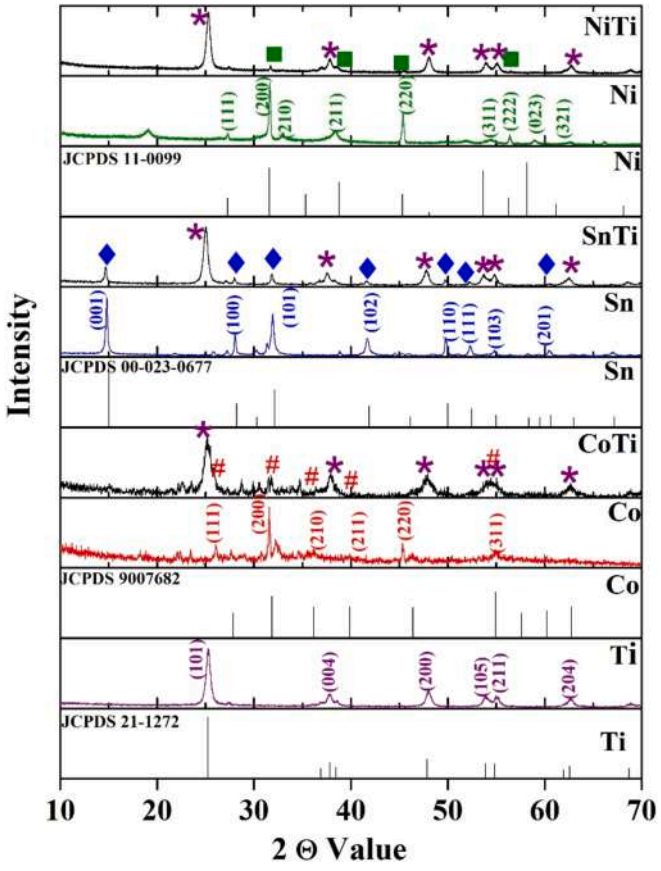

Fig. 2. XRD patterns for Ti, Co, 10-CoTi, Sn, 10-SnTi, Ni, and 10-NiTi.

hydrogen evolution reaction takes place through three major steps [13,14]. The first step absorption of light by catalyst to eject the electron to conduction band and the formation of hole in valence band; in the second step, exciton pair are separated would migrate to the reactive

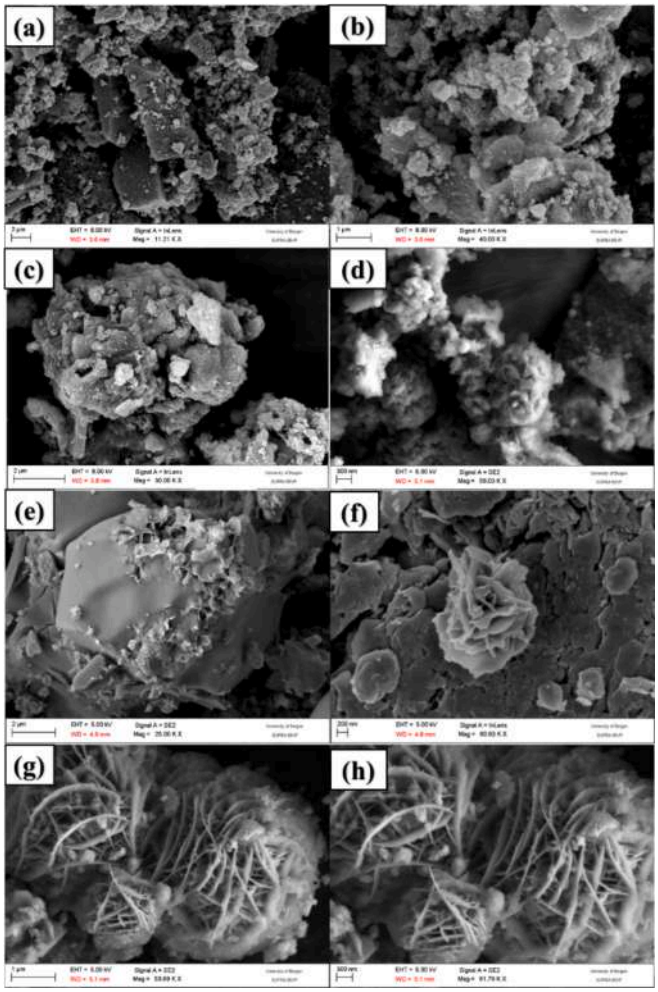

Fig. 3. SEM images for pure TiO_2 (a, b), 10-CoTi (c, d), 10-NiTi (e, f), and 10-SnTi (g, h).

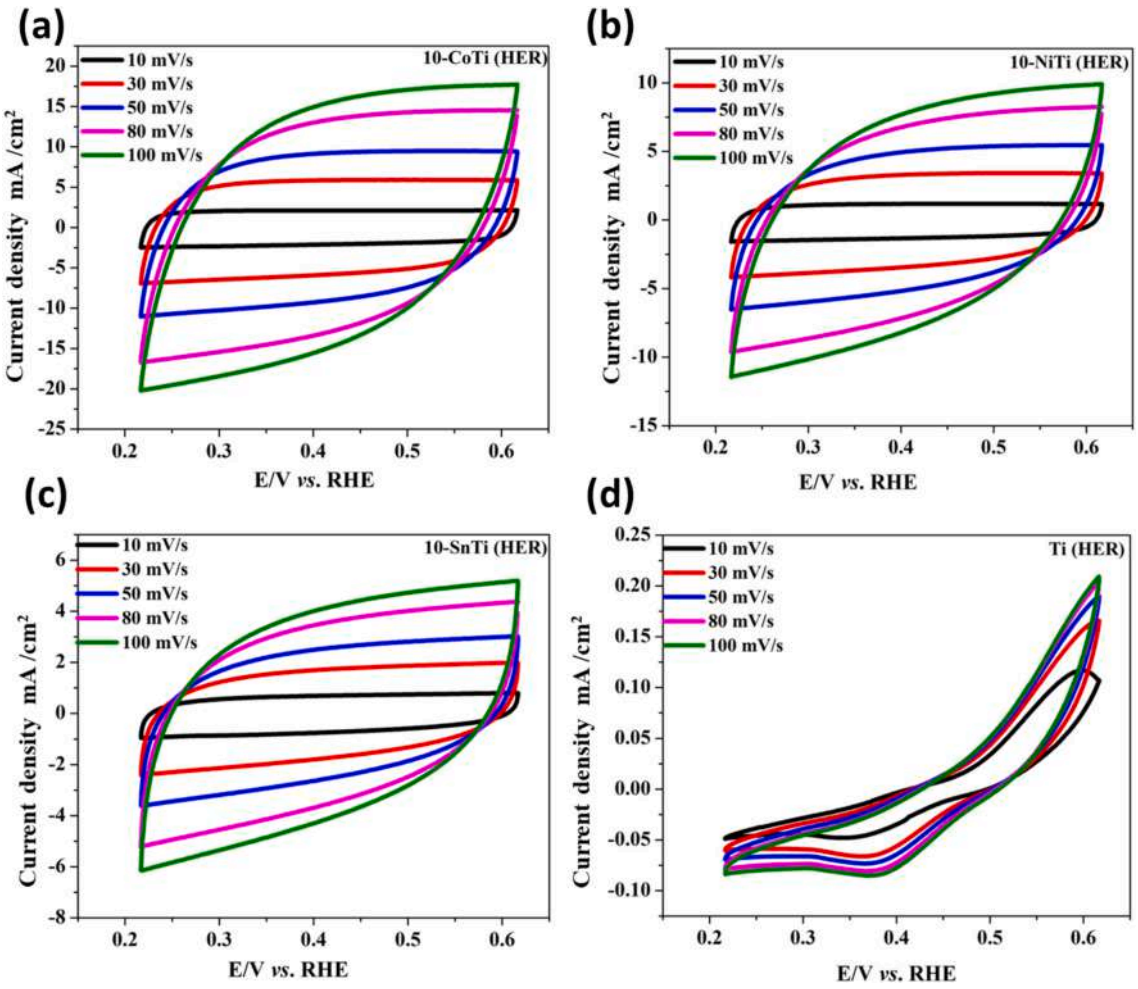

Fig. 4. CV profile (a) 10-CoTi (b) 10-NiTi (c) 10-SnTi nanocomposites and (d) Ti for HER.

sites. Finally, in the third step, surface reactions take place, i.e. electrons reduce the hydrogen ion from the water molecule and produce hydrogen gas, whereas holes reduce the oxygen ions an produce oxygen gas [15,16].

Electrochemical water splitting involves two half reactions, hydrogen evolution (HER) and oxygen evolution (OER) reactions that concludes overall water splitting reaction [9]. In essence, the electrochemical reaction is straightforward but is limited by slow moving kinetics on the oxygen evolution side and hydrogen evolution side. Therefore, recently various advanced electrocatalysts have been innovated to provide an adequate active site for hydrogen production and to reduce the overpotential of HER and OER [17,18]. Platinum (Pt)-based electrocatalysts are the most efficient catalysts, but the scarcity of Pt and its high cost limit their commercial use [19–22]. Much research is currently focused on developing non-precious metal-based catalysts for these reactions, primarily transition metal oxides [23–27] or hydroxides [28], and metal organic framework derived metal oxy hydroxides [29] for OER and transition metal chalcogenides (TMC) [30,31], phosphines [32] and MXenes (two-dimensional thin layer transition metal carbides or nitrides) [23,33] for HER.

TMC materials have become interesting materials in electrochemical, photocatalytic hydrogen evolution, photodegradation and energy storage (lithium ion batteries, supercapacitors) applications [34].

In previous studies [35–37] different weight percentage of CoS_2/TiO_2, SnS_2/TiO_2 and NiS_2/TiO_2 materials were utilized in the powder form for photocatalytic hydrogen evolution. These studies showed that 10 wt% of MS_2/TiO_2 materials exhibited the optimal photocatalytic activity. Moreover, in another study, these materials were tested for photocatalytic hydrogen evolution in seawater [38]. Therefore, previous research has demonstrated that these materials are potential candidates for photocatalytic hydrogen production. To scale up and reuse the materials, this study develops electrodes with a coating of these materials on a substrate and investigates their potential for both photocatalytic and electrocatalytic hydrogen production. We focus on three different transition metal chalcogenide-embedded titanium dioxide nanocomposite materials coated on FTO, namely MS_2/TiO_2 (M = Co, Sn and Ni) nanocomposites.

2. Materials and method

2.1. Materials

Unless otherwise stated all the materials were utilized without further purification. Titanium isopropoxide, 98+% (Sigma-Aldrich Norway AS, Oslo, Norway) was employed as the precursor for TiO_2 preparation, Cobalt (II) nitrate hexahydrate, 99 % pure (Sigma-Aldrich Norway AS) was utilized as the cobalt precursor. $SnCl_2{\cdot}2H_2O$ (ACS reagent, ≥98 % (Sigma–Aldrich Norway AS)) was used as the tin precursor, and $NiCl_2$ anhydrous (Sigma–Aldrich Norway AS) was used as the nickel precursor; $Na_2S_2O_3$, Na_2S (Sigma-Aldrich Norway AS) and thiourea, ACS reagent, 99.0 % (Sigma–Aldrich Norway AS) were used as sulfur sources. PHARMCO-AAPER Ethyl alcohol (200 Proof; Absolute, anhydrous, Sigma-Aldrich Norway AS) was used as solvent, con. HCl (used as a hydrolyser) and deionized water (resistivity >18 Wcm) was used to prepare the solution mixtures.

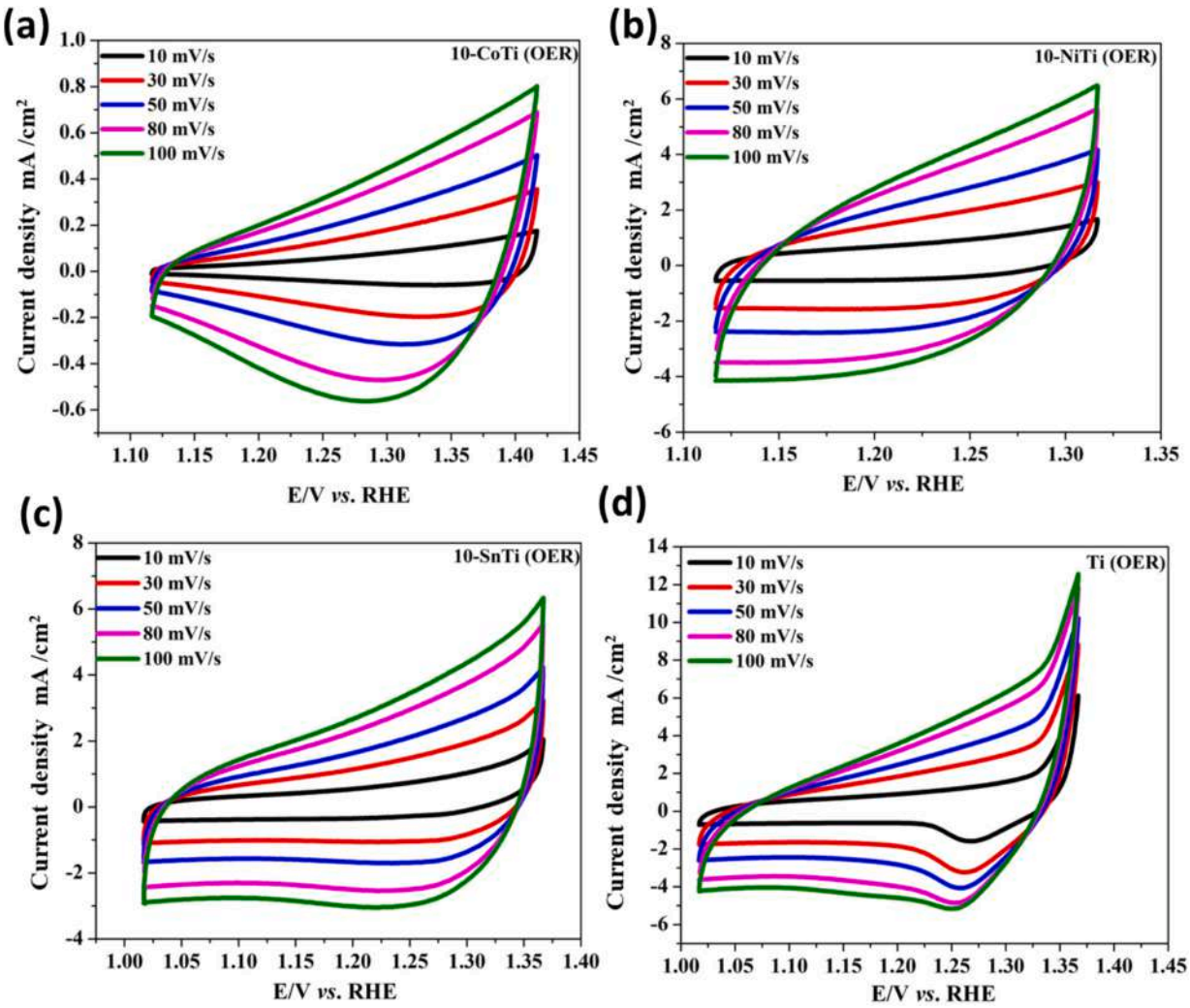

Fig. 5. CV profile (a) 10-CoTi (b) 10-NiTi (c) 10-SnTi nanocomposites and (d) Ti for OER.

Table 1
Comparison of specific capacitance value of MS_2/TiO_2 nanocomposites and pristine TiO_2 nanocrystalline materials.

Materials	Specific capacitance (F/g) @ 10 mV/s	
	HER	OER
10-CoTi	65.7	0.88
10-SnTi	21.4	14.3
10-NiTi	38.2	18.8
Ti	0.47	27.8

2.2. Methods

2.2.1. Synthesis of TiO_2

TiO_2 nanocrystalline material was synthesized by combined sol–gel and hydrothermal method refer as previous study [35]. 0.3 mL of Con HNO_3 was poured in 32.5 mL of absolute ethanol and the mixture was stirred well. 6.5 mL of titanium tetra isopropoxide (TTIP) were added in to the above solution drop wise. Finally, 3 mL of water was added in to it. The resulting gel was transferred into an autoclave and kept at 150 °C for 6 h. Finally, the product was washed with ethanol and annealed at 500 °C for 6 h.

Our previous studies [35–37] showed that 10 wt% of MS_2/TiO_2 materials were the optimal photocatalytic activity of the material, thus we focused on synthesizing this particular weight percentage in this study.

2.2.2. Synthesis of 10 wt% of CoS_2/TiO_2

Appropriate amount of $Co(NO_3)_2$ and $Na_2S_2O_3$ were added in to a 100 mL aqueous solution containing deionized water and ethanol in 2:1 ratio under constant stirring (300 rpm) for 30 min. Finally, required amount of TiO_2 (hydrothermally synthesized) was dispersed into above solution and the resulting mixture was hydrothermally treated at 180 °C to prepare 10 wt% of CoS_2 embedded TiO_2 material [35].

2.2.3. Synthesis of 10 wt% of SnS_2/TiO_2

The appropriate amount of $SnCl_2{\cdot}2H_2O$ was taken into a 50 mL beaker and acidified with 0.8 mL of concentrated hydrochloric acid (37 %) in 10 mL of deionized water. The solution mixture was then stirred at 300 rpm for 30 min followed by the addition of the appropriate amount of TiO_2 (hydrothermally synthesized) to completely disperse by constant stirring for 10 min. Then, an appropriate amount of thiourea was added into the solution made up to 40 mL volume by adding deionized water. Finally, the resulting solution was transferred in an autoclave and kept at 145 °C for 12 h. The final product was collected by centrifugation and washed with the mixture of deionized water and ethanol (v/v = 1:1) several times. Finally, the product was air-dried [36].

2.2.4. Synthesis of 10 wt% of NiS_2/TiO_2

Appropriate amount of $NiCl_2$ was taken in a beaker containing 40 mL of water. Appropriate amount of TiO_2 (hydrothermally synthesized) was

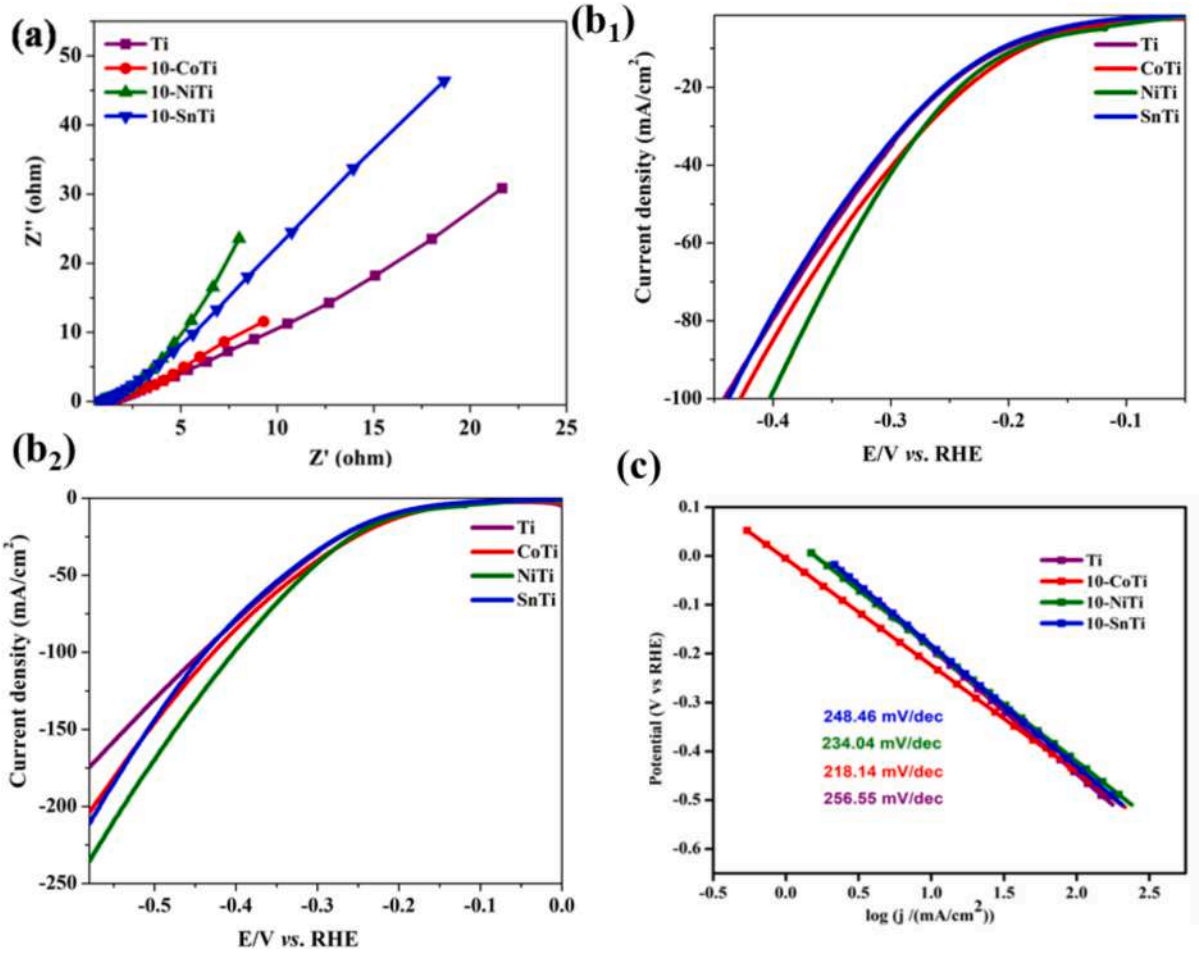

Fig. 6. (a) EIS spectra, (b) LSV profile (c) Tafel slope of Ti, 10-CoTi, 10-NiTi and 10-SnTi nanocomposites for HER.

Table 2
Solution resistance values of Ti, 10-CoTi, 10-NiTi and 10-SnTi nanocomposites electrodes for OER and HER.

Materials	Resistance values (Ω)-Rs	
	HER	OER
10-CoTi	0.921	0.831
10-NiTi	0.845	0.743
10-SnTi	0.847	1.703
Ti	1.336	1.258

dispersed into the above solution by sonication for 10 min at 50 °C. Then, Na_2S was added into it and stirred well. The resultant mixture was transferred into an autoclave and kept at 140 °C for 10 h. The product was collected and centrifuged at 2500 rpm for 2 min and washed with ethanol and air-dried.

The synthesized materials were referred as follows; TiO_2 = Ti, 10 wt % CoS_2/TiO_2 = 10-CoTi, 10 wt% NiS_2/TiO_2 = 10-NiTi and 10 wt% SnS_2/TiO_2 = 10-SnTi.

2.3. Characterization

Synthesized nanocomposite materials were characterized using different techniques, such as powder X-ray diffraction (patterns of the catalysts were recorded using D8 ADVANCE ECO in a 1 kW copper X-ray tube diffractometer with the scan range from 3 to 90 degrees (2theta)), diffuse reflectance spectra (DRS Cary 100 Bio UV–Visible spectrophotometer, Santa Clara, CA, USA) by measuring the intensity in the wavelength range of 800–200 nm, and scanning electron microscopy (SEM, ZEISS SUPRA 55VP Field emission. KV range: 100 V til 30 kV).

2.4. Electrochemical measurements

The entire electrochemical measurements were carried out by using biologic SP 150 workstation at room temperature in three electrode system. 1 M KOH was used as the electrolyte for the electrochemical cell. The working electrode was made up with the material, activated carbon, and polyvinylidene fluoride (PVDF) binder with a weight percentage of 70 %, 20 % and 10 % respectively. The mentioned materials were grounded as slurry by using n-methyl pyrollidone (NMP) as solvent. Resulted slurry was coated on Ni foam and the electrochemical measurements such as Cyclic Voltammetry (CV), Linear sweep voltammetry (LSV), electrochemical impedance spectroscopy (EIS) and Chronoamperometry (CA) studies were performed. In OER process, Ag/AgCl and platinum was used as reference and counter electrodes, respectively. Similarly, Ag/AgCl and graphite rod was used as reference and counter electrodes in the HER process, respectively.

2.5. Hydrogen evolution experiment

The photocatalytic experiments were conducted using pristine TiO_2, and MS_2/TiO_2 (M = Co, Sn and Ni) nanocomposites. First, the synthesized nanocomposite was coated onto a 4×4 cm^2 FTO glass plate and immersed in a solution containing 70 mL of deionized water and 10 mL of methanol (as a hole scavenger). The setup was degassed for 60 min with high-purity nitrogen prior to irradiation (as illustrated in Fig. 1). A 150 W Xenon lamp (Oriel light source, Xenon arc lamp, Scientific Instruments) was used as the irradiation source. The amount of H_2

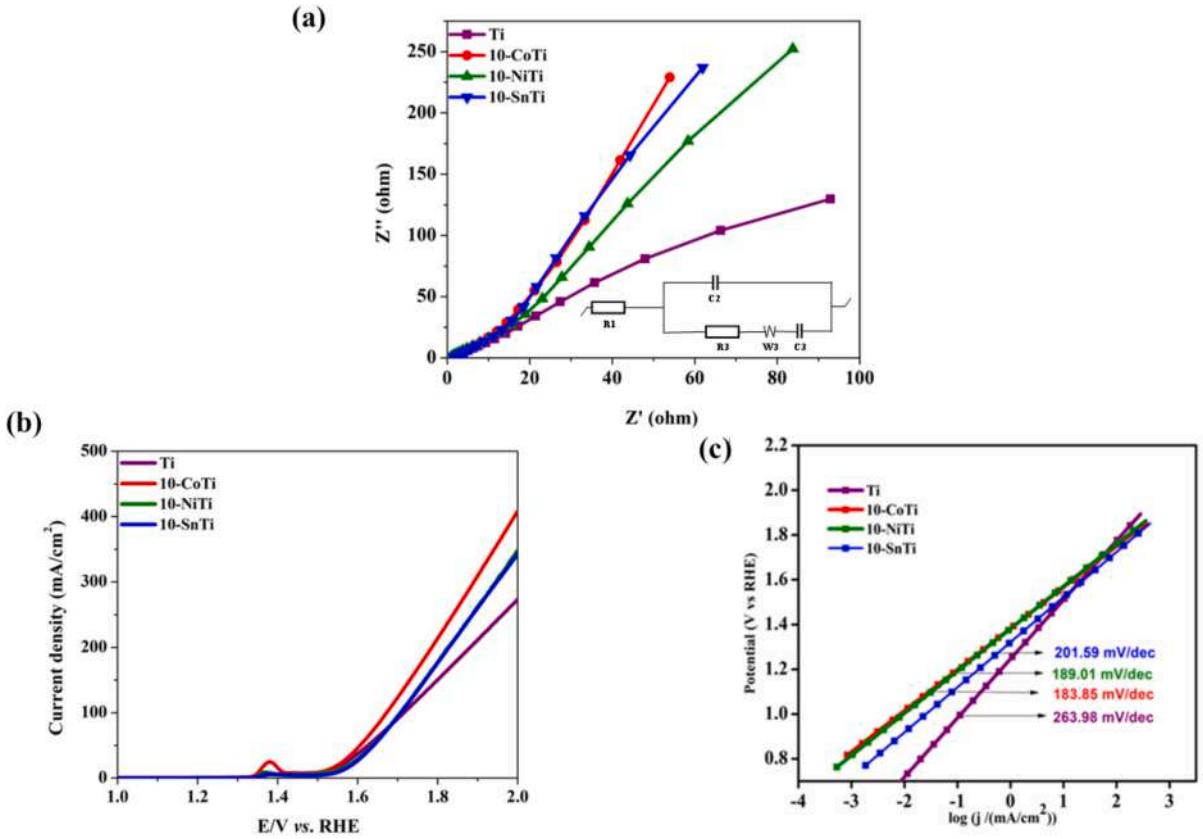

Fig. 7. (a) EIS spectra, (b) LSV profile (c) Tafel slope of Ti, 10-CoTi, 10-NiTi and 10-SnTi nanocomposites for OER.

Table 3
The current density, overpotential, and Tafel slope values of 10-CoTi, 10-NiTi, 10-SnTi and Ti nanocomposites electrodes for OER and HER.

Material	Current Density (mA/cm^2)		Over potential (mV)		Tafel slope (mV/dec)	
	OER	HER	OER	HER	OER	HER
10-CoTi	406.4 mA/cm^2	−202.3 mA/cm^2	280 mV	185 mV	183.85 mV/dec	218.14 mV/dec
10-NiTi	346.8 mA/cm^2	−233.4 mA/cm^2	315 mV	189 mV	189.01 mV/dec	234.04 mV/dec
10-SnTi	337.3 mA/cm^2	−209.7 mA/cm^2	322 mV	204 mV	201.59 mV/dec	248.46 mV/dec
Ti	271.1 mA/cm^2	−172.5 mA/cm^2	293 mV	200 mV	263.98 mV/dec	256.55 mV/dec

Table 4
ECSA values of 10-CoTi, 10-NiTi, 10-SnTi and Ti nanocomposites electrodes for HER and OER.

Materials	ECSA (cm^2)	
	HER	OER
10-CoTi	131.45	511.625
10-NiTi	28.975	195.750
10-SnTi	42.425	175.100
Ti	22.550	201.625

produced was measured by using gas chromatography (Trace 1300, Thermo scientific) equipped with a molecular sieve column and a thermal conductivity detector (TCD), and the amount of hydrogen produced was quantified by using a calibration curve prepared previously.

Similarly, the amount of hydrogen generated during the electrochemical reaction was calculated using the same method while applying an external circuit voltage, with a 1 M KOH solution as electrolyte.

3. Results and discussion

The XRD patterns confirmed the formation of the nanoparticles (Fig. 2). The structural quality and phase orientation for synthesized nanocomposite between the 20° to 70° diffraction angles confirmed the presence of chalcogenide and TiO_2 phases in the resultant materials. Anatase phase formation along with the crystal plane orientations evaluated by the diffraction angles 25.50°, 37.76°, 48.10°, 53.88°, 55.84° and 62.90° related to the planes of (101), (004), (200), (105), (211) and (204), respectively authenticated from JCPDS number (JCPDS 21-1272) [39]. The CoS_2 phase formation with the two-theta degree angles of 26.04°, 31.58°, 37.08°, 40.34°, 45.34° and 55.1° are due to (111), (200), (210), (211), (220) and (311) diffraction planes of CoS_2, respectively correlated with the JCPDS Card No: 9007682. The peaks at 2 theta values of 14.76, 27.97, 32.00, 41.79, 49.92, 52.41, 54.79, and 60.55° for pristine SnS_2 are due to (001), (100), (101), (102), (110), (111), (103), and (201) diffraction planes, respectively confirm the formation of SnS_2 (JCPDS:00-023-0677). The peaks obtained at the 2 theta values of 27.29, 31.63, 33.00, 38.304, 45.37, 54.49, 56.41, 59.02 and 62.52° due to (111), (200), (210), (211), (220), (311), (222), (023) and (321) diffraction planes, respectively for pure NiS_2, which matches with (JCPDS 11-0099).

Combinations of the peaks for MS_2 and TiO_2 were observed in the 10 wt% of MS_2/TiO_2 nanocomposite materials, confirming the impregnation of MS_2 in TiO_2 nanocrystalline. The absence of any other peaks for oxides or any other compounds in the XRD of all the tested samples further confirms the purity of the obtained nanocomposite materials [38].

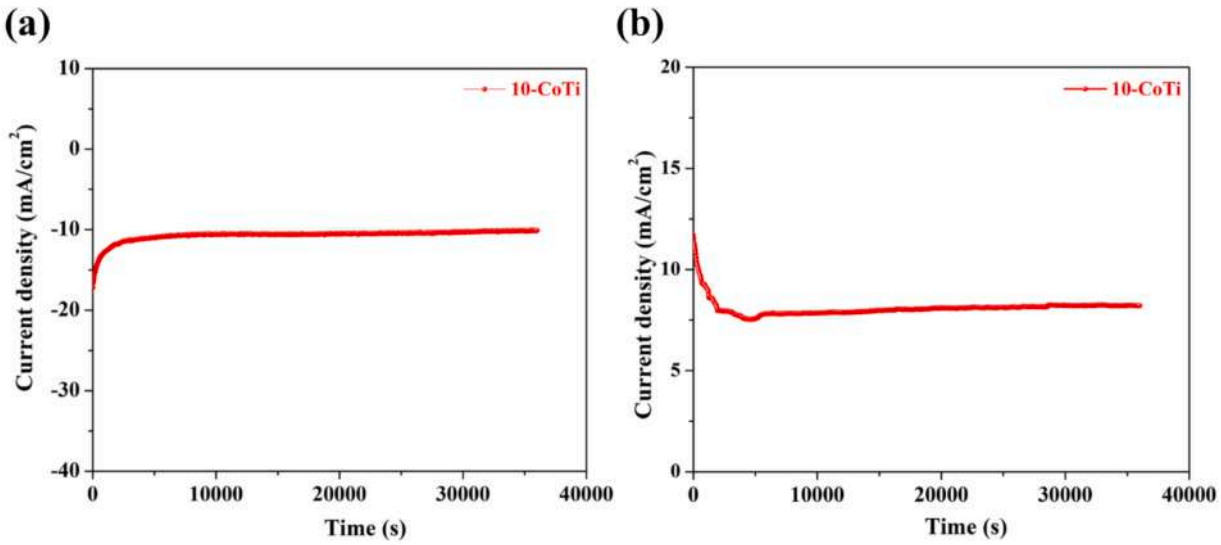

Fig. 8. (a) Chronoamperometry test at 10 h for 10-CoTi nanocomposite, HER, and (b) OER.

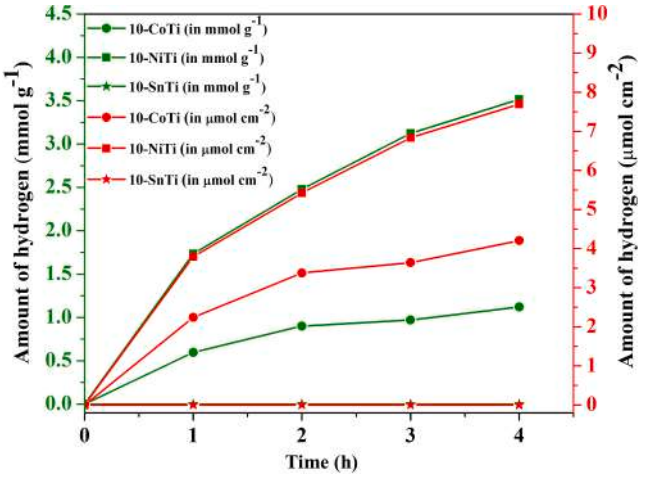

Fig. 9. Amount of hydrogen evolution from photocatalysis of 10-CoTi, 10-NiTi and 10-SnTi nanocomposites over extended solar irradiation.

Table 5
Comparison of amount of hydrogen evolution in photocatalysis where the materials used in a powder form as a suspension and coated film as an electrode.

Material	Amount of H_2 evolution in photocatalysis after 4 h light illumination (mmol/g)	
	Suspension (previous study)	Electrode (This work)
10-CoTi	2.55 [35]	1.12
10-NiTi	3.60 [37]	3.52

Fig. 3 shows the scanning electron microscope images of for pure TiO_2 (3(a, b)), 10-CoTi (3(c, d)), 10-NiTi (3(e, f)), and 10-SnTi (3(g, h)). An irregular 3D block-like structure covered with spongy like particles was attained for TiO_2 nanocomposite and is shown in Fig. 3a and 3b. It can be clearly seen that the aggregated particles have spongy like structures. The mixed composite, 10-CoTi also exhibits the aggregation, and it shows rod like structure covered with spongy like particles (Fig. 3c and 3d).

The images of 10-NiTi nanocomposites are shown in Fig. 3e and 3f. These NiS_2/TiO_2 nanocomposites possess flake like structure that form a flower with sponge-like material and, thus, possess aggregation. SEM images of 10-SnTi nanocomposites, shown in Fig. 3g and 3 h. These SnS_2/TiO_2 nanocomposites possess flower like structure decorated with sponge-like material and, therefore, exhibit aggregation. Additionally, the atomic ratios of Ni/Sn/Co:S:Ti:O were obtained using energy-dispersive spectroscopy (EDS), as shown in Fig. S1. The surface area measurements, referenced from previous studies [38], were obtained using Brunauer–Emmett–Teller (BET) analysis. The calculated surface area of Ti, 10-SnTi, 10-NiTi and 10-CoTi are 107.233, 100.934, 44.563 and 105.391 m^2/g, respectively. These materials are classified as type IV isotherm according to the IUPAC classification, with all materials exhibiting mesoporous characteristics. The pore sizes of Ti, 10-SnTi, 10-NiTi and 10-CoTi are 8.322 nm, 8.098 nm, 8.275 nm and 8.291 nm, respectively, all within the range of 2–50 nm. The surface areas of these nanocomposites are smaller than pristine TiO_2, likely due to the agglomeration of nanoparticles, which may reduce the surface area by increasing the particle size. The observed loss in surface area and decrease in pore diameter can be attributed to the incorporation of transition metal chalcogenide species into the mesoporous structure. The results shows that photocatalysts with mesoporous structure can create impurity bands in the bandgap, acting as trapping centres for photo-induced charge carriers and promoting the interfacial charge transfer process [38,40].

The electrochemical HER and OER half reactions, of the synthesized MS_2/TiO_2 nanocomposites coated in Ni form electrode were studied under different electrochemical characterizations that include cyclic voltammetry (CV), Electrochemical Impedance Spectroscopy (EIS), Linear sweep voltammetry (LSV) and Tafel slope in aqueous alkaline 1 M KOH under three electrode system. CV graphs of 10-CoTi, 10-SnTi, 10-NiTi and Ti materials for HER and OER as illustrated in Fig. 4. andFig. 5. show the pseudocapacitive nature of those electrodes.

Oxidation and reduction behavior were analyzed with respect to scan rates, 10, 30, 50, 80 and 100 mV/s. The potential windows maintained for HER and OER were 1.0–1.50 V *vs* RHE and 0.2–0.6 V *vs.* RHE, respectively. The specific capacitance of the nanocomposites are calculated using, $C = \frac{\int IdV}{ms(V2-V1)}$ where IdV is the area under the CV curve; m is the mass of the material coated in Ni foam; s is the scan rate; and $(V2-V1)$, is the potential window.

The calculated specific capacitance values of OER and HER for the materials are given in Table 1. 10-CoTi, 10-SnTi, and 10-NiTi nanocomposites electrodes clearly show higher specific capacitance behavior in HER in nanocomposites than in pure Ti material (Table 1). As with HER, similar CV behavior was observed with OER, but Ti shows to have

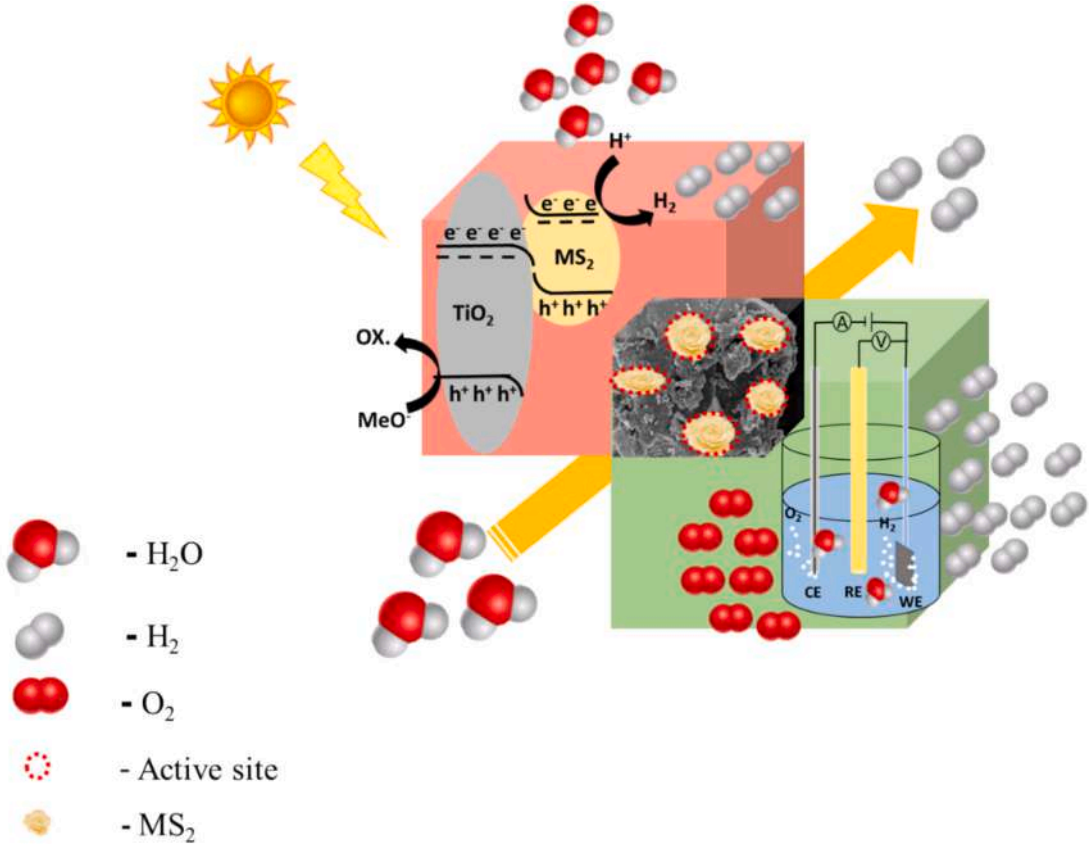

Fig. 10. Proposed Schematic diagram of the band configuration and charge separation at the MS_2/TiO_2 heterojunction.

higher specific capacitance values than the nanocomposites during the OER. These results clearly show that morphology of the nanocomposites assists enhancing its active sites by improving surface properties [24] as indicated elsewhere.

EIS spectra of the synthesized materials depicted in Fig. 6a, and 7a reveals the conducting behavior of materials and their charge transfer ability. Here, the frequency range was kept at 100 mHz to 100 kHz. From these data, it can be proved that the charge transfer and internal facilitation of the electrode resulted with better conductive ability of the electrode. Solution resistances are calculated from the graph and tabulated in Table. 2. It clearly shows that the composite electrodes have much lower internal resistance during the electrochemical reaction compared to the bare titania electrode, resulting in higher conductivity.

The water oxidation and reduction ability of these electrodes were studied by using linear sweep voltammetry (LSV) at the alkaline condition, and the potentials were set as 0–(-0.6) V and 1.0–2.0 V for HER (Fig. 6b) and OER (Fig. 7b) reactions, respectively. Over potentials for water oxidation and reduction reactions were (Table 3) compared to Ti nanomaterial, lower potential values were achieved for 10-CoTi (185 and 280 mV) nanocomposite, 10-NiTi (189 and 315 mV), and 10-SnTi (204 and 322 mV) nanocomposites for HER and OER, respectively.

The best current densities of -233.4 mA/cm^2 for HER by the 10-NiTi and 406.4 mA/cm^2 for OER by the 10-CoTi electrode were attained at a scan rate of 10 mV/s. The higher electrochemical activity of these electrodes for oxidation and reduction may be attributed to the morphology of the nanocomposites that results in enhanced surface property, and thus, higher number of active sites. Conductivity of combined electrode with lower over potential adhered with more current density one of the main features for the selection of efficient electrodes for HER, OER or overall water splitting applications.

Using the LSV data, the Tafel slopes (Fig. 6c and 7c) were plotted for every electrode and the values are shown in Table 3 which analyses the reaction rate succeeded by the electrode during the water splitting reactions. It is one of main property to inherent the HER and OER. Tafel slopes were plotted according to the equation.

$$\eta = b\log j + a$$

where, j is current density; a is the fitting parameter; b is the Tafel slope, and η is over potential [24]. The Tafel values of the electrodes are found to be 218.14, 234.04, 248.46, and 256.55 mV/dec, for 10-CoTi, 10-NiTi, 10-SnTi, and Ti for HER respectively, and 183.85, 189.01, 201.59 and 263.98 mV/dec for 10-CoTi, 10-NiTi, 10-SnTi and Ti for OER respectively. A lower value of Tafel slope obtained by electrode of nanocomposites for HER and OER compared with Ti material indicates the faster HER and OER rate, which may be due to the large number of electrons involve in the electrochemical reactions [41,42]. The uniform and rapid photocurrent response was observed in both Pure TiO_2 and MS_2/TiO_2 electrodes and the photo responsive phenomenon was entirely reversible under simulated solar irradiation (Fig. S2). The higher current density was observed with MS_2/TiO_2 compared to pure TiO_2, indicating that our design is feasible. The significant difference between these photoelectrode likely due to effective light absorbance, and electron transfer in the composite materials.

Electrochemical active surface area (ECSA) was calculated to investigate the electrochemical interfacial area of synthesized product in the non-redox region, as illustrated in Figs. S3 and S4. Using following equations [26],

$$\mathrm{ECSA} = \frac{C_{dl}}{C_s} \quad (1)$$

Where the C_{dl}- Double layer capacitance, C_s- Specific capacitance of substrate

Double layer capacitance values were determined across various electrochemical regions. ECSA is proportional to C_{dl}. The C_{dl} values were

approximated by plotting current density $\Delta j = \frac{(j_a - j_b)}{2}$, ($j_a$ and j_b represents the current densities in CV) against different scan rates (10–100 mVs^{-1}) at a fixed potential of 0.85 V *vs.* RHE for HER and, 1.27 V *vs.* RHE for OER. The calculated ECSA values for the 10-CoTi, 10-NiTi, 10-SnTi and Ti nanocomposites electrodes for HER and OER are shown in Table 4. The higher ECSA was obtained for 10-CoTi material, which leads to improved electrocatalytic activity. Therefore, excellent HER and OER activity were achieved with this nanocomposite due to the beneficial structural features [43].

The durability of 10-CoTi nanocomposite material was tested by chronoamperometry analysis for 10 h. It demonstrated continuous hydrogen evolution at 10 mA/cm^2 and remained constant throughout the entire 10-hour test period, as shown in Fig. 8a. The results indicate that it is a highly effective catalyst for HER in alkaline medium. Similarly, Fig. 8b shows that the potential of 10-CoTi electrode remained constant for 10 h during OER testing. The results revealed that the catalyst is also effective for OER performance in alkaline media.

Additionally, when comparing the amount of hydrogen produced during the electrochemical reaction (using H-cell photoelectrochemical reactor), the MS_2/TiO_2 electrodes shows greater amount than pure titania electrode (Fig. S5).

The amount of hydrogen evolution during the photocatalytic and electrocatalytic process were analysed using the experimental method described in Fig. 1. Hydrogen production was measured as 0.946 $mmolcm^{-2}$, 0.886 $mmolcm^{-2}$, 0.808 $mmolcm^{-2}$, and 0.278 $mmolcm^{-2}$ for 10-NiTi, 10-CoTi, 10-SnTi and Ti nanomaterials, respectively in the electrocatalytic process. For the photocatalytic process, 10-NiTi, and 10-CoTi produced 7.69 $\mu molcm^{-2}$ (3.52 $mmolg^{-1}$) and 4.21 $\mu molcm^{-2}$ (1.12 $mmolg^{-1}$) of hydrogen, respectively using MS_2/TiO_2 coated in FTO glasses under 4 h solar light illumination (Fig. 9). In contrast, 10-SnTi and Ti nanomaterials show no hydrogen production in this process.

Table 5 shows a comparison of hydrogen evolution in photocatalytic reaction for 10-CoTi, 10-NiTi and 10-SnTi composites, as reported in our previous studies [35–37], along with the new results here when these materials are used as coated electrodes. The amount of hydrogen produced using 10-CoTi catalyst was almost the same whether it was used in the powder form or as electrodes. The same phenomenon was observed for 10-NiTi; however, in the case of 10-SnTi, as mentioned, there was no significant hydrogen production when this material was used as an electrode.

The maximum amount of hydrogen evolution was obtained with 10-NiTi nanocomposite material in both methods. It can be attributed to both electron–hole separation and scavenging ability of these processes. Additionally, the catalytic activity can be correlated with the bandgap of these materials (Bandgap 10-CoTi-3.4 eV, 10-NiTi-1.7 eV, 10-SnTi-2.1 eV, Ti-3.2 eV referred previous studies [35,36,38]).

Although the 10-CoTi exhibits similar bandgap to Ti, better electron-hole separation at the active site, facilitated by a heterojunction [44], may result in improved performance for 10-CoTi. Optimal hydrogen evolution was recorded with 10-NiTi. In the case of pure MS_2 (Band gap <2.5 eV), it can be concluded that the rapid recombination of photo generated excitons hinders the hydrogen formation. However, MS_2 act as co-catalyst in the composite (MS_2/TiO_2), enhancing the hydrogen production by effectively absorbing visible light and exciting more electrons at the active site.

These results lead to a proposed mechanism as illustrated in the schematic model, where it is projected that the conduction bands and valence bands of the different counterparts are in a “staggered form” (Fig. 10). Under light illumination, the excited electrons in MS_2, with a lower conduction band (CB), could recombine with the holes in TiO_2, which has a higher valence band (VB) in the two contacted semiconductors. This interaction induces the loss of some photo-generated electrons to some extent and resulting in higher efficiency.

4. Conclusion

Through this study, we have clearly demonstrated that electrodes made of transition metal chalcogenide-embedded titanium dioxide (MS_2/TiO_2, M = Co, Ni, and Sn) nanocomposites are highly promising candidates for electrocatalytic and photocatalytic hydrogen evolution reactions. The nanocomposites were successfully synthesized using facile hydrothermal method, and their electrochemical and photocatalytic performance were studies under different experimental conditions.

- 10-NiTi showed an optimum current density of 233.4 mA/cm^2 in OER, while 10-CoTi exhibited a current density of 406.4 mA/cm^2 in the HER process.
- Lower overpotential values of 280 mV and 185 mV were obtained in the OER and HER with the 10-CoTi nanomaterial compared with other materials.
- Low Tafel slope values of 183.85 and 218.14 mV/dec were measured for the 10-CoTi nanomaterial.
- Hydrogen production during the electrocatalytic process was 0.946 $mmolcm^{-2}$, 0.886 $mmolcm^{-2}$, 0.808 $mmolcm^{-2}$, and 0.278 $mmolcm^{-2}$, for 10-NiTi, 10-CoTi, 10-SnTi and Ti nanomaterials, respectively.
- In the photocatalytic process, 10-NiTi, and 10-CoTi produced 7.69 $\mu molcm^{-2}$ (3.52 $mmolg^{-1}$) and 4.21 $\mu molcm^{-2}$ (1.12 $mmolg^{-1}$) of hydrogen, respectively using MS_2/TiO_2 coated on FTO glasses under 4 h of solar light illumination.
- MS_2 materials act as co-catalyst, effectively absorbing photons, and serving as reactive sites for efficient catalytic performance by capturing electrons from the exciton pairs.

Our results indicate that when transition metal chalcogenide-embedded titanium dioxide (MS_2, M = Co, Ni, and Sn) nanocomposites are used as electrodes, amount of hydrogen evolution from electrocatalysis is higher than that from the photocatalysis process. This study illustrates that upscaling green hydrogen production through electrocatalysis and photocatalysis processes will be feasible with MS_2/TiO_2 nanocomposite electrodes.

CRediT authorship contribution statement

Sivagowri Shanmugaratnam: Writing – original draft, Validation, Software, Methodology, Investigation, Formal analysis, Data curation, Conceptualization. **Swathi Srinivasan:** Writing – review & editing, Validation, Formal analysis. **Rathinam Yuvakkumar:** Writing – review & editing, Validation. **Velaug Myrseth Oltedal:** Writing – review & editing. **Punniamoorthi Ravirajan:** Writing – review & editing, Supervision, Project administration, Funding acquisition. **Yohi Shivatharsiny:** Writing – review & editing, Validation, Supervision, Methodology, Investigation, Data curation, Conceptualization. **Dhayalan Velauthapillai:** Writing – review & editing, Validation, Supervision, Resources, Project administration, Funding acquisition.

Declaration of competing interest

The authors declare that they have no known competing financial interests or personal relationships that could have appeared to influence the work reported in this paper.

Acknowledgements

Grant number NORPART2021/10095 “Higher education and Research collaboration on Nanomaterials for Clean Energy Technologies 2.0 (HRNCET 2.0) and Research Council of Norway (RCN) Project number: 333151 - Center for Environment-friendly Research (FME) HyValue - Norwegian center for hydrogen value chain research.

Appendix A. Supplementary data

Supplementary data to this article can be found online at https://doi.org/10.1016/j.fuel.2024.134101.

Data availability

Data will be made available on request.

References

[1] Som NN, Jha PK. Hydrogen evolution reaction of metal Di-chalcogenides: ZrS_2, $ZrSe_2$ and Janus ZrSSe. Int J Hydrogen Energy 2019;45:23920–7. https://doi.org/10.1016/j.ijhydene.2019.09.033.

[2] Kakoulaki G, Kougias I, Taylor N, Dolci F, Moya J. Green Hydrogen in Europe – A Reg Assess : Substit Exist Prod Elect Powered by Renewables 2021;228. https://doi.org/10.1016/j.enconman.2020.113649.

[3] Shanmugaratnam S, Yogenthiran E, Koodali R, Ravirajan P, Velauthapillai D, Shivatharsiny Y. Recent Progress Approach Trans Metal Chalcogenides for Hydrogen Product 2021:1–37. https://doi.org/10.1016/S1872-2067(17)62956-5.

[4] Dincer I. Green methods for hydrogen production. Int J Hydrogen Energy 2012;37:1954–71. https://doi.org/10.1016/j.ijhydene.2011.03.173.

[5] Atilhan S, Park S, El-halwagi MM, Moore M, Nielsen RB. ScienceDirect green hydrogen as an alternative fuel for the shipping industry. Curr Opin Chem Eng 2021;31:100668. https://doi.org/10.1016/j.coche.2020.100668.

[6] E.T. Dolf Gielen, and R.M. (IRENA).; Available *HYDROGEN : A RENEWABLE*; International Renewable Energy Agency, Abu Dhabi About, 2019; ISBN 9789292601515.

[7] Dawood F, Anda M, Shafiullah GM. ScienceDirect hydrogen production for energy : An overview. Int J Hydrogen Energy 2019;45:3847–69. https://doi.org/10.1016/j.ijhydene.2019.12.059.

[8] Kuang Y, Kenney MJ, Meng Y, Hung W, Liu Y, Solar-Driven EJ. Highly sustained splitting of seawater into. Hydrogen and Oxygen Fuels 2019;1–6:doi:10.1073/pnas.1900556116.

[9] Du X, Zhang X, Yang Z, Gong Y. Water oxidation catalysis beginning with $CuCo_2S_4$: Investigation of the true electrochemically driven catalyst. Chem - An Asian J 2018;13:266–70. https://doi.org/10.1002/asia.201701684.

[10] Yano J, Grauer DC, Long JR, Liu C, Chang CJ, Yang P, et al. Electrodeposited cobalt-sulfide catalyst for electrochemical and photoelectrochemical hydrogen generation from water. J Am Chem Soc 2013;135:17699–702. https://doi.org/10.1021/ja4094764.

[11] Khan S, Je M, Nu N, Ton T, Lei W, Taniike T. Environmental C-doped ZnS-ZnO / Rh nanosheets as multijunctioned photocatalysts for effective H_2 generation from pure water under solar simulating light. Appl Catal B Environ 2021;297:120473. https://doi.org/10.1016/j.apcatb.2021.120473.

[12] Gusain M, Dubey A, Das M, Singh SK. Facial surfactant-free hydrothermal synthesis of MoS_2 Microflower and its effect in electrochemical properties. J Solid State Chem 2019;274:58–63. https://doi.org/10.1016/j.jssc.2019.03.010.

[13] Kudo A, Miseki Y. Heterogeneous photocatalyst materials for water splitting. Chem Soc Rev 2009;38:253–78. https://doi.org/10.1039/b800489g.

[14] Kudo A, Kato H, Tsuji I. Strategies for the development of visible-light-driven photocatalysts for water splitting. Chem Lett 2004;33:1534–9. https://doi.org/10.1246/cl.2004.1534.

[15] Leung DYC, Fu X, Wang C, Ni M, Leung MKH, Wang X, et al. Hydrogen production over titania-based photocatalysts. ChemSusChem 2010;3:681–94. https://doi.org/10.1002/cssc.201000014.

[16] Ge L, Han C, Xiao X, Guo L. Synthesis and characterization of composite visible light active photocatalysts MoS_2-g-C_3N_4 with enhanced hydrogen evolution activity. Int J Hydrogen Energy 2013;38:6960–9. https://doi.org/10.1016/j.ijhydene.2013.04.006.

[17] Yao N, Tan T, Yang F, Cheng G, Luo W. Well-aligned metal-organic framework array-derived CoS_2 nanosheets toward robust electrochemical water splitting. Mater Chem Front 2018;2:1732–8. https://doi.org/10.1039/c8qm00259b.

[18] Li Y, He B, Liu X, Hu X, Huang J, Ye S, et al. Graphene confined MoS_2 particles for accelerated electrocatalytic hydrogen evolution. Int J Hydrogen Energy 2019;44:8070–8. https://doi.org/10.1016/j.ijhydene.2019.02.089.

[19] Nguyen VT, Le PA, Hsu YC, Wei KH. Plasma-induced exfoliation provides onion-like graphene-surrounded MoS_2 nanosheets for a highly efficient hydrogen evolution reaction. ACS Appl Mater Interfaces 2020;12:11533–42. https://doi.org/10.1021/acsami.9b20902.

[20] Li G, Chen Z, Li Y, Zhang D, Yang W, Liu Y, et al. Engineering substrate interaction to improve hydrogen evolution catalysis of monolayer MoS_2 films beyond Pt. ACS Nano 2020;14:1707–14. https://doi.org/10.1021/acsnano.9b07324.

[21] Ke X, Dai K, Zhu G, Zhang J, Liang C. In situ photochemical synthesis noble-metal-free NiS on CdS-diethylenetriamine nanosheets for boosting photocatalytic H_2 production activity. Appl Surf Sci 2019;481:669–77. https://doi.org/10.1016/j.apsusc.2019.03.171.

[22] Wiensch JD, John J, Velazquez JM, Torelli DA, Pieterick AP, McDowell MT, et al. Comparative study in acidic and alkaline media of the effects of PH and Crystallinity on the hydrogen-evolution reaction on MoS_2 and $MoSe_2$. ACS Energy Lett 2017;2:2234–8. https://doi.org/10.1021/acsenergylett.7b00700.

[23] Yang JX, Yu WB, Li CF, Dong Da W, Jiang LQ, Zhou N, Zhuang ZP, Liu J, Hu ZY, Zhao H, et al. PtO nanodots promoting Ti3C2 MXene in-situ converted Ti_3C_2/TiO_2 composites for photocatalytic hydrogen production. Chem Eng J 2021;420. https://doi.org/10.1016/j.cej.2021.129695.

[24] Rani BJ, Ravi G, Ravichandran S, Ganesh V, Ameen F, Al-Sabri A, et al. Electrochemically active XWO_4 (X = Co, Cu, Mn, Zn) nanostructure for water splitting applications. Appl Nanosci 2018;8:1241–58. https://doi.org/10.1007/s13204-018-0780-2.

[25] Hussain M, Abu El Maati L, Alomar MA, Ali M, Abdullah M, Aman S, et al. Improvement of $SnFe_2O_4$ OER electrochemical property by Sm doping for water splitting. Ceram Int 2024;50:19525–33. https://doi.org/10.1016/j.ceramint.2024.03.050.

[26] Aman S, Ahmad N, Tahir MB, Alanazi MM, Abdelmohsen SAM, Khosa RY, et al. Understanding the spatial configurations of Sm_2O_3 in NiO interfaces embedded-loaded for electrocatalytic OER process. Surf Interfaces 2023;38:102857. https://doi.org/10.1016/j.surfin.2023.102857.

[27] Gouadria S, Abudllah M, Ahmad Z, John P, Nisa MU, Manzoor S, et al. Development of bifunctional Mo doped $ZnAl_2O_4$ spinel nanorods array directly grown on carbon fiber for supercapacitor and OER application. Ceram Int 2023;49:4281–9. https://doi.org/10.1016/j.ceramint.2022.09.312.

[28] Xue BW, Zhang CH, Wang YZ, Xie WW, Li N. Nanoscale advances recent progress of Ni – Fe layered double hydroxide and beyond towards electrochemical. Water 2020:5555–66. https://doi.org/10.1039/d0na00727g.

[29] Alburaih HA, Manzoor S, Abdullah M, Ashiq MN, Aman S, Trukhanov SV, et al. Electro-oxidation reconstitution of aluminium copper MOF-Derived metal oxyhydroxides for a robust OER process. RSC Adv 2023;13:8736–42. https://doi.org/10.1039/d2ra07661f.

[30] Ma F, Liang Y, Zhou P, Tong F, Wang Z, Wang P, et al. One-step synthesis of Co-doped 1T-MoS_2 nanosheets with efficient and stable HER activity in alkaline solutions. Mater Chem Phys 2020;244:122642. https://doi.org/10.1016/j.matchemphys.2020.122642.

[31] Merki D, Fierro S, Vrubel H, Hu X. Amorphous Molybdenum sulfide films as catalysts for electrochemical hydrogen production in water. Chem Sci 2011:1262–7. https://doi.org/10.1039/c1sc00117e.

[32] Wondimu TH, Chen G, Kabtamu DM, Chen H, Bayeh AW, Huang H, et al. Highly efficient and durable phosphine reduced iron-doped tungsten oxide / reduced graphene oxide nanocomposites for the hydrogen evolution reaction. Int J Hydrogen Energy 2018;43:6481–90. https://doi.org/10.1016/j.ijhydene.2018.02.080.

[33] Qiao J, Kong L, Xu S, Lin K, He W, Ni M, et al. Research progress of MXene-based catalysts for electrochemical water-splitting and metal-air batteries. Energy Storage Mater 2021;43:509–30. https://doi.org/10.1016/j.ensm.2021.09.034.

[34] Sivagowri Shanmugaratnam, Shivatharsiny, R. *Transition Metal Chalcogenide (TMC) Nanocomposites for Environmental Remediation Application over Extended Solar Irradiation*; 2012; doi: 10.1016/j.colsurfa.2011.12.014.

[35] Shanmugaratnam S, Velauthapillai D, Ravirajan P, Christy AA, Shivatharsiny Y. CoS_2/TiO_2 in Nanocomposites for hydrogen production under UV irradiation. Materials (Basel) 2019;12:doi:10.3390/MA12233882.

[36] Shanmugaratnam S, Selvaratnam B, Baride A, Koodali R, Ravirajan P, Velauthapillai D, et al. SnS_2/TiO_2 nanocomposites for hydrogen production and photodegradation under extended solar irradiation. Catalysts 2021;11:1–12. https://doi.org/10.3390/catal11050589.

[37] Shanmugaratnam S, Ravirajan P, Yohi S, Velauthapillai D. Well-separated photoinduced charge carriers on hydrogen production using NiS_2/TiO_2 nanocomposites. ACS Omega 2023. https://doi.org/10.1021/acsomega.3c08194.

[38] Shanmugaratnam S, Ravirajan P, Shivatharsiny Y, Velauthapillai D. Green hydrogen production through photocatalytic seawater splitting on MS_2/TiO_2 (M=Ni/Co/Sn) nanocomposites over simulated solar irradiation. Int J Hydrogen Energy 2024;91:673–82. https://doi.org/10.1016/j.ijhydene.2024.10.091.

[39] Xing J, Li YH, Jiang HB, Wang Y, Yang HG. The size and valence state effect of pt on photocatalytic H 2 evolution over platinized TiO_2 photocatalyst. Int J Hydrogen Energy 2014;39:1237–42. https://doi.org/10.1016/j.ijhydene.2013.11.041.

[40] Lin HY, Shih CY. Efficient one-pot microwave-assisted hydrothermal synthesis of M (M = Cr, Ni, Cu, Nb) and nitrogen Co-doped TiO_2 for hydrogen production by photocatalytic water splitting. J Mol Catal A Chem 2015;411:128–37. https://doi.org/10.1016/j.molcata.2015.10.026.

[41] Shinagawa T, Garcia-Esparza AT, Takanabe K. Insight on tafel slopes from a microkinetic analysis of aqueous electrocatalysis for energy conversion. Sci Rep 2015;5:1–21. https://doi.org/10.1038/srep13801.

[42] Khan SB, Kamal T, Asiri AM, Bakhsh EM. Iron doped nanocomposites based efficient catalyst for hydrogen production and reduction of organic pollutant. Colloids Surfaces A Physicochem Eng Asp 2021;608:125502. https://doi.org/10.1016/j.colsurfa.2020.125502.

[43] Swathi S, Yuvakkumar R, Ravi G, Thambidurai M, Arunmetha S, Velauthapillai D. Nanoplatelets assembled $CuCo_2S_4$/N doped RGO nanocomposites for hydrogen evolution reaction. Int J Hydrogen Energy 2024;65:704–16. https://doi.org/10.1016/j.ijhydene.2024.03.148.

[44] Xu, M.; Ye, T.; Dai, F.; Yang, J.; Shen, J.; He, Q. Rationally Designed n – n Heterojunction with Highly Efficient Solar Hydrogen Evolution. 1–9, doi:10.1002/cssc.201403334.